



Supplementary Information for
Rate of atmospheric brown carbon whitening governed by
environmental conditions

Elijah G. Schnitzler^{a,1,2}, Nealan G. A. Gerrebos^{b,1}, Therese S. Carter^c, Yuanzhou Huang^b, Colette L. Heald^{c,d,3}, Allan K. Bertram^{b,3}, and Jonathan P. D. Abbatt^{a,3}

^aDepartment of Chemistry, University of Toronto, Toronto, M5S 3H6, Canada; ^bDepartment of Chemistry, University of British Columbia, Vancouver, V6T 1Z1, Canada; ^cCivil and Environmental Engineering Department, Massachusetts Institute of Technology, Cambridge, 02139, USA; ^dEarth, Atmospheric and Planetary Sciences, Massachusetts Institute of Technology, Cambridge, 02139, USA

¹E.G.S. and N.G.A.G. contributed equally to this work.

²Present address: Department of Chemistry, Oklahoma State University, Stillwater, 74078, USA

³To whom correspondence may be addressed. Email: jonathan.abbatt@utoronto.ca, bertram@chem.ubc.ca, or heald@mit.edu.

This PDF file includes:

Supplementary text
Figures S1 to S13
Table S1 and S2
SI References

Supplementary Information Text

S1. Viscosity Parameterization. The experimental viscosity data points, including the viscosity of pure water, were fit to the following equation to give a parameterization of viscosity as a function of RH at 294 K, $\log[\eta(RH, 294 K)]$:

$$\log(\eta(RH, 294K)) = \left(\left(\frac{\left(1 + \kappa \left(\frac{a_w}{1-a_w}\right)^{-1}\right) \left(\frac{1}{MW_{BBOA}}\right)}{\left(1 + \kappa \left(\frac{a_w}{1-a_w}\right)^{-1}\right) \left(\frac{1}{MW_{BBOA}}\right) + \left(1 - \left(1 + \kappa \left(\frac{a_w}{1-a_w}\right)^{-1}\right) \left(\frac{1}{MW_{H_2O}}\right)\right)} \right) * \log(\eta_{BBOA,dry}) \right) + \left(\left(1 - \left(\frac{\left(1 + \kappa \left(\frac{a_w}{1-a_w}\right)^{-1}\right) \left(\frac{1}{MW_{BBOA}}\right)}{\left(1 + \kappa \left(\frac{a_w}{1-a_w}\right)^{-1}\right) \left(\frac{1}{MW_{BBOA}}\right) + \left(1 - \left(1 + \kappa \left(\frac{a_w}{1-a_w}\right)^{-1}\right) \left(\frac{1}{MW_{H_2O}}\right)\right)} \right) \right) * \log(\eta_{H_2O}) \right) \quad [S1]$$

where a_w is the water activity (RH/100), κ is a mass-based hygroscopicity parameter used to fit the equation to the experimental data, $\eta_{BBOA,dry}$ is the viscosity of the dry BBOA material corresponding to the experimental results at 0% RH, η_{H_2O} is the viscosity of pure water, 10^{-3} Pa s (1), MW_{BBOA} is the average molecular weight of the BBOA molecules, and MW_{H_2O} is the molecular weight of water, 18.015 g mol⁻¹. Eq. **S1** was derived by substituting Eq. **S3** and **S4**, below, into Eq. **S2**, the mole fraction-based Arrhenius mixing rule (2, 3):

$$\log(\eta_{BBOA,wet}) = \chi_{BBOA} \log(\eta_{BBOA,dry}) + (1 - \chi_{BBOA}) \log(\eta_{H_2O}) \quad [S2]$$

where $\eta_{BBOA,wet}$ is the viscosity of the BBOA-water mixture and χ_{BBOA} denotes the mole fraction of BBOA in the BBOA-water mixture. Eq. **S3** relates the mole-fraction of BBOA, χ_{BBOA} , to the weight fraction of the BBOA, w_{BBOA} :

$$\chi_{BBOA} = \frac{\frac{w_{BBOA}}{MW_{BBOA}}}{\frac{w_{BBOA}}{MW_{BBOA}} + \frac{1-w_{BBOA}}{MW_{H_2O}}} \quad [S3]$$

Eq. **S4** relates w_{BBOA} to a mass-based hygroscopicity parameter, κ (4):

$$w_s = \left(1 + \kappa \frac{a_w}{1-a_w}\right)^{-1} \quad [S4]$$

MW_{BBOA} was assumed to be 248 g mol⁻¹, based on the range of molecular weights, 138–358 g mol⁻¹, of BrC molecules observed in BBOA from pine trees (5).

To account for varying temperature, a parameterization for viscosity as a function of both RH and temperature was determined using the Vogel-Fulcher-Tamman (VFT) equation, as done previously (6, 7):

$$\eta(RH, T) = \eta_{\infty} e^{\frac{T_0(RH)D_f}{T - T_0(RH)}} \quad [S5]$$

where η_{∞} is the viscosity at infinite temperature, 10^{-5} Pa s (8, 9), D_f is the fragility parameter, assumed to be 10 (7, 10), and $T_0(RH)$ is the RH-dependent Vogel temperature. $T_0(RH)$ was calculated by rearranging Eq. **S5** and evaluating at 294 K.

$$T_0(RH) = \frac{\ln\left(\frac{\eta(RH,294\text{ K})}{\eta_\infty}\right)294\text{ K}}{D_f + \ln\left(\frac{\eta(RH,294\text{ K})}{\eta_\infty}\right)} \quad [\text{S6}]$$

Once the Vogel temperature was determined, viscosity as a function of RH and temperature was calculated with Eq. **S5**.

S2. Time Scale Analysis of the Mixing Time of BrC within the Particles in the Laboratory Experiments. To determine if there was a gradient in BrC within the particles during the laboratory experiments we calculated the mixing time of BrC within the particles ($\tau_{\text{mix,BrC}}$) using the following equation (11):

$$\tau_{\text{mix,BrC}}(RH, T) = \frac{d_p^2}{4\pi^2 D_{\text{BrC}}(RH, T)} \quad [\text{S7}]$$

where d_p is the particle diameter and D_{BrC} is the diffusion coefficient of the organic molecules in the particle. D_{BrC} was calculated using the parameterization for viscosity as a function of RH and temperature and the fractional Stokes-Einstein equation (12):

$$D_{\text{BrC}}(RH, T) = D_{\text{BrC},0}(T) \left(\frac{\eta_0(T)}{\eta_{\text{BrC}}(RH, T)}\right)^\xi \quad [\text{S8}]$$

where D_{BrC} is the diffusion rate of BrC, $D_{\text{BrC},0}$ is the diffusion rate of BrC in pure water, calculated with the standard Stokes-Einstein equation, η_0 is the viscosity of water, η_{BrC} is the viscosity of the BrC particles, and ξ is the fractional exponent calculated, as done previously (12). The viscosity of water was calculated as a function of temperature (see Eq. **S14**) (6). The fractional exponent, ξ , was calculated with the following equation (12):

$$\xi = 1 - \left(A e^{\left(-B \frac{R_{\text{BrC}}}{R_{\text{matrix}}}\right)} \right) \quad [\text{S9}]$$

where $A = 0.73$, $B = 1.79$, R_{BrC} is the hydrodynamic radius of BrC, and R_{matrix} is the average hydrodynamic radius of the molecules in the BBOA particles – which in this case is assumed to be equivalent to BrC, so $\frac{R_{\text{BrC}}}{R_{\text{matrix}}} = 1$. With these parameters, $\xi = 0.878$.

Shown in Fig. S11 (Panel B) are the $\tau_{\text{mix,BrC}}$ values calculated with Eq. **S7**. Also included in Fig. S11 (Panel A) are the relative absorption measurements for the laboratory experiments as a function of RH at 253, 273 and 293 K after exposure to 45 ppm of ozone for 130 s. Fig. S11 illustrates that the mixing time of BrC within the particles in the laboratory experiments is at least a factor of 20 smaller than the reaction time in the laboratory experiments (130 s) for all cases when significant reactivity of the BrC was observed (relative absorption < 0.9). This timescale analysis implies that there was not a steep gradient in the BrC in laboratory experiments when there was significant reactivity of the BrC.

S3. Kinetic Analysis. Eq. **1** can be rewritten in terms of ozone partial pressure, P_{O_3} , as in Morris et al. (13).

$$\sqrt{\frac{[\text{BrC}](t)}{[\text{BrC}]_0}} = 1 - \frac{3H\sqrt{D_{O_3}k_2}}{2a\sqrt{[\text{BrC}]_0}} P_{O_3} t \quad [\text{S10}]$$

The fraction of BrC that remains unreacted is obtained by rearranging Eq. **S10**. The fraction of BrC unreacted is assumed to be equivalent to the absorption relative to the initial absorption since the reaction bleaches BrC:

$$\frac{[\text{BrC}]_t}{[\text{BrC}]_0} \cong \frac{Ab_t}{Abs_0} = \left(1 - \frac{3H\sqrt{D_{O_3}k_2}}{2a\sqrt{[\text{BrC}]_0}} P_{O_3} t \right)^2 \quad [\text{S11}]$$

The experimental results show that the absorption of BrC never falls below approximately 50% of the initial value, regardless of RH or temperature. Eq. 2 is obtained from Eq. S11 to reflect this feature, forcing Abs_t/Abs_0 to stay $\geq 50\%$.

D_{O_3} was calculated using the parameterization for viscosity as a function of RH and temperature and the fractional Stokes-Einstein equation:

$$D_{O_3}(RH, T) = D_{O_3,0}(T) \left(\frac{\eta_0(T)}{\eta_{BBOA}(RH, T)} \right)^\xi \quad [S12]$$

where D_{O_3} is the diffusion rate of ozone in the particles, $D_{O_3,0}$ is the diffusion rate of ozone in pure water, calculated with the standard Stokes-Einstein equation, η_0 is the viscosity of water, η_{BBOA} is the viscosity of the BBOA particles, and ξ is the fractional exponent calculated, as done previously (12). The viscosity of water was calculated as a function of temperature (6). The fractional exponent, ξ , is calculated with the following equation (12):

$$\xi = 1 - \left(A e^{\left(-B \frac{R_{O_3}}{R_{matrix}} \right)} \right) \quad [S13]$$

where $A = 0.73$, $B = 1.79$, R_{O_3} is the hydrodynamic radius of ozone, and R_{matrix} is the average hydrodynamic radius of the molecules in the BBOA particles (i.e., the matrix). For R_{O_3} , 0.198 nm is used, based on the van der Waals radii using atomic increments (12). For the R_{matrix} , 0.423 nm is used, based on the assumed molecular weight (248 g mol⁻¹) and density (1.3 g cm⁻³) and assuming spherical symmetry of the molecules (5, 14, 15). With these parameters, $\xi = 0.684$. The viscosity of water as a function of temperature is calculated using Eq. S14:

$$\log(\eta_0) = A + \frac{B}{(T - T_0)} \quad [S14]$$

where $A = -4.28$, $B = 152.87$ and $T_0 = 173.06$ K (6).

When fitting Eq. 2 to the experimental data in Fig. 1A and 1B, we assume D_{O_3} is a function of temperature and RH, and $H(k_2/[BrC]_0)^{1/2}$ is a function of temperature and independent of RH. The data in Fig. 1A and Fig. S7 is consistent with this assumption.

S4. Estimated $H(k_2/[BrC]_0)^{1/2}$ Values Based on the Literature. To estimate $H(k_2/[BrC]_0)^{1/2}$ values we first estimated H, k_2 , and $[BrC]_0$ values based on the literature. To estimate $[BrC]_0$ we first assumed that the concentration of organic molecules in biomass burning aerosol particles was 5.2 M, based on a molecular weight of 248 g mol⁻¹ (5) and a density of 1.3 g cm⁻³ (14, 15). Of these organic molecules, only a fraction will be BrC. For the sake of this calculation, we assume the fraction was between roughly 1 and 10 %. However, we note that this estimate is particularly hard to make given that some small fraction of the aerosol (e.g. the alkene, highly conjugated component) may be strongly absorbing and reactive, whereas a larger fraction (e.g. the functionalized aromatic component) may be both moderately absorbing and reactive. This results in $[BrC]_0$ values between 0.52 M and 0.052 M.

Values of H at room temperature for O₃ in pure oleic acid, decane, and water are 4.8×10⁻¹ M atm⁻¹, 1.8×10⁻² M atm⁻¹, and 1.0×10⁻² M atm⁻¹, respectively (16–18). A recent study by Berkemeier et al. 2016 estimated that the H value for ozone in shikimic acid is 1.8×10⁻¹ M atm⁻¹ and 4.0×10⁻² M atm⁻¹ at RH values of 0% and 92% at 23 °C (18). Since shikimic acid is likely similar to some of the organic molecules in biomass burning organic aerosol, we use these values as estimates of H as a function of RH for O₃ in biomass burning aerosol particles at room temperature.

Listed in Table S2 are second order rate constants at room temperature for the reaction between O₃ and different types of organic molecules with structures similar to molecules expected for BrC. Based on these values, we estimate that the second order rate constant between O₃ and different types of organics relevant for BrC is roughly between 9×10⁻² and 4.7×10⁵ M⁻¹ s⁻¹.

Based on the information above, we estimate that $H(k_2/[BrC]_0)^{1/2}$ values are between 7.5×10⁻² and 5.4×10² atm⁻¹ s^{-1/2} at 0% RH and between 1.7×10⁻² and 1.2×10² atm⁻¹ s^{-1/2} at 92% RH at room temperature. This range is consistent with the values extracted from our fits at room temperature (see Fig. S7), which are between 3.8×10⁰ and 1.6×10¹ atm⁻¹s^{-1/2}.

S5. Model Representation Assuming the Reaction between O₃ and BrC was Limited by Only Diffusion of BrC within the Particles. According to the resistor model, if the reaction between ozone and BrC occurs at the surface and is limited only by diffusion of BrC to the surface, the reactivity of BrC within the particle can be described by the following equation:

$$\ln \frac{[BrC](t)}{[BrC]_0} = \frac{12D_{BrC}}{a^2} t \quad \text{[S15]}$$

Where D_{BrC} is the diffusion coefficient of BrC, a is the particle radius and t is the time. The absorption of BrC in the ozonolysis experiments never fell below approximately 50% of the original value, so Eq. S15 was rearranged and constrained to fit these observations.

$$\frac{[BrC](t)}{[BrC]_0} \approx \frac{Abs_t}{Abs_0} = EXP\left(\frac{12D_{BrC}}{a^2} t\right) * 0.5 + 0.5 \quad \text{[S16]}$$

Where Abs_t/Abs_0 is the absorption relative to the initial absorption, Eq. S16 was used to predict the relative absorption of BrC as a function of RH at temperatures of 253, 273, and 293 K (Fig. S12). For t and a , values of 130 s and 143 nm were used, based on the residence time and median volume radius of the particles used in the flow tube experiments. D_{BrC} was calculated using the parameterization for viscosity as a function of RH and temperature and the fractional Stokes-Einstein equation (12), as discussed in the SI Appendix (section S2). Shown in Fig. S12 is a comparison of the predictions of Eq. S16 with the experimental data for the relative absorption at 405 nm as a function of RH at 293, 273, and 253 K. For these experiments, $P_{O_3} = 4.5 \times 10^{-5}$ atm (45 ppm). For this case, the agreement between the experimental data and the predictions was poor. Furthermore, this model representation assumes the kinetics are independent of O₃ concentrations, which is not consistent with our experimental measurements (main text, Fig. 1B).

S6. Model Representation Assuming O₃ and BrC Were Well-Mixed throughout the Particles. According to the resistor model, if O₃ and BrC are well-mixed throughout the particles (i.e., no concentration gradients), the reactivity of BrC can be described by the following equation:

$$\ln \left(\frac{[Br](t)}{[BrC]_0} \right) = -HP_{O_3} k_2 t \quad \text{[S17]}$$

The absorption of BrC in the ozonolysis experiments never fell below approximately 50% of the original value, so the equation was rearranged and constrained to fit these observations.

$$\frac{[Br](t)}{[BrC]_0} \approx \frac{Abs_t}{Abs_0} = e^{-HP_{O_3} k_2 t} * 0.5 + 0.5 \quad \text{[S18]}$$

If we assume the product Hk_2 is an exponential function of RH, we were able to describe the experimental data reasonably well with Eq. S18 (Fig. S13A). However, the Hk_2 values determined from the fit (Fig. S13B) were not consistent with expectations. For example, at room temperature, the Hk_2 values from the fit imply that Hk_2 increases by more than an order of magnitude when going

from 10 to 70 % RH. In contrast, literature data suggests that Hk_2 should decrease with an increase in RH (SI Appendix, Section S4). The solubility of O_3 in water is less than that of O_3 in organics so particles with higher water content should take up less O_3 , as confirmed by experiments in the literature (16–18). The reaction rate coefficient, on the other hand, is not expected to be affected by the RH. In other words, good agreement between the experimental data and Eq. 18 was only obtained if unrealistic values of H and k_2 were assumed.

S7. Sample Conditioning for Whitening Experiments. Filter samples were soaked in 50 mL of ultrapure water (18.2 M Ω cm). The extracts were passed through a syringe filter with 0.45- μ m pore size (Whatman), and then transferred to an atomizer (Topas, ATM 226). The atomizer was supplied by lab air, and an activated carbon filter (Whatman, Carbon Cap 150) was placed at the air inlet. A fraction of the output of the atomizer, at a flow rate of 0.8 L min⁻¹, was used as the sample, and the remainder was exhausted, as shown in Fig. S1. The sample was directed through a diffusion denuder packed with granular activated carbon (Sigma-Aldrich, 4-14 mesh) to remove semi-volatile organic constituents. To obtain a certain RH, a fraction of the sample flow was then passed through a diffusion dryer packed with indicating silica gel (EMD Millipore, 6-18 mesh) and re-introduced before the combined streams were directed into a mixing volume.

The resulting submicron particles, with a geometric mean diameter of about 100 nm, were introduced into a reaction flow tube with precise control of temperature, relative humidity, and ozone mixing ratio, as discussed in the Materials and Methods section. Downstream of the reaction flow tube, the sample was passed through a diffusion denuder packed with granular catalyst (Carus, Carulite 200) to remove ozone, limiting reaction to the flow tube. The sample was then passed through a second diffusion dryer. The size distribution of BBOA was measured using a scanning mobility particle sizer (SMPS), consisting of a soft X-ray aerosol neutralizer (TSI, 3087), a long differential mobility analyzer (DMA; TSI, 3776), and a condensation particle counter (CPC; TSI, 3776). The absorption and scattering coefficients of the BBOA were measured using a photoacoustic soot spectrometer (PASS; Droplet Measurement Technologies), equipped with lasers at 405 and 781 nm and a reciprocal integrating nephelometer. The second diffusion dryer ensured that the size distributions and absorption and scattering coefficients were measured for dry particles.

S8. Fluid Dynamic and Viscosity Simulation. Fluid dynamic simulations were performed using COMSOL Multiphysics (Version 5.2a) software. Details regarding pore-flow simulations have been reported previously (19) and were discussed briefly in the Materials and Methods section. The simulations required the following inputs: dimensions of the droplet, surface tension of the material, density of the material, slip length (a measure of resistance to flow at the hydrophobic glass surface), and contact angle between the droplet and the hydrophobic glass surface. The dimensions of the droplets used in the simulations were the same as in the experiments. The other inputs used in the simulations are listed in Table S1.

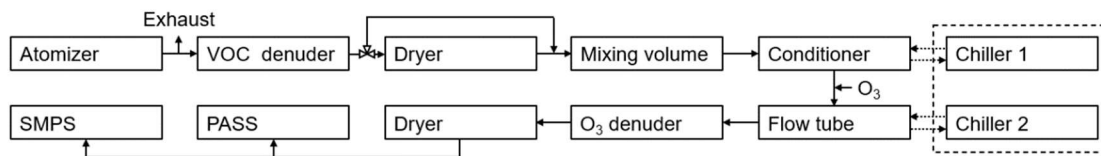


Fig. S1. Experimental setup for the generation, pre-treatment, and RH- and temperature-controlled heterogeneous oxidation of water-soluble BBOA. PASS: photo-acoustic soot spectrometer; SMPS: scanning mobility particle sizer.

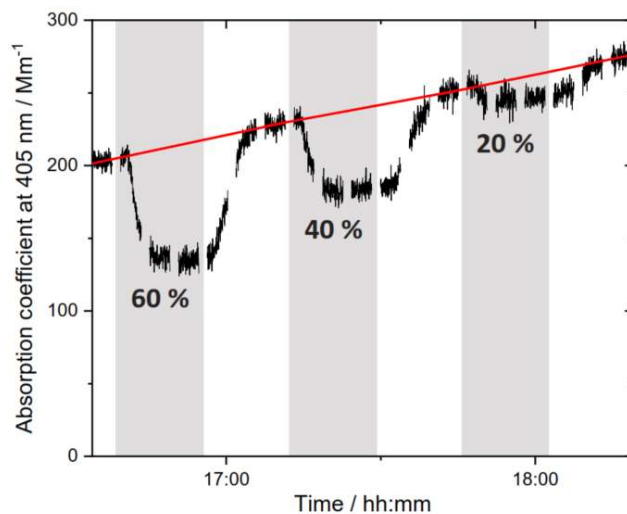


Fig. S2. Time series of the absorption coefficient at 405 nm of water-soluble BBOA alternately in the absence and presence (indicated with grey bars) of 45 ppm of ozone at 273 K and 20-60% RH. The absorption coefficient at 405 nm in the absence of ozone increased gradually during each experiment, possibly due to the solution in the atomizer becoming more concentrated over time as particles were nebulized. However, this increase had no effect on the observed reactivities; two sets of data without systematic variation were collected sequentially for each BBOA extract, one as RH was increasing, another as RH was decreasing, all while the solution slowly became more absorptive.

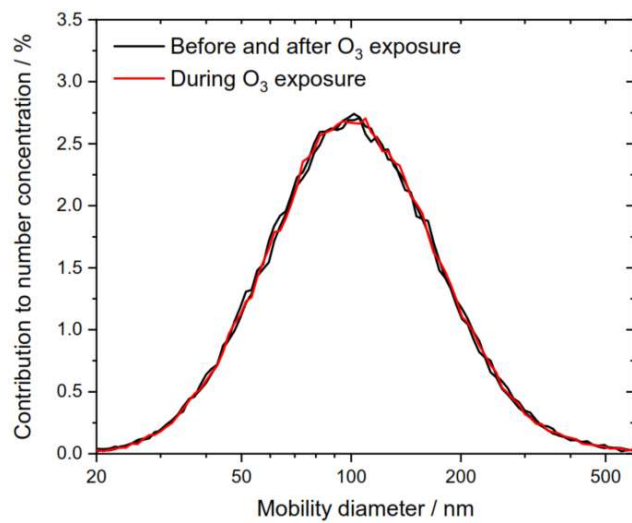


Fig. S3. Size distributions of water-soluble BBOA before, during, and after ozone exposure at 273 K and 60% RH are indistinguishable.

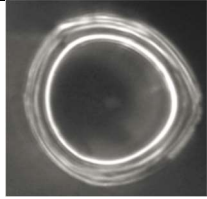




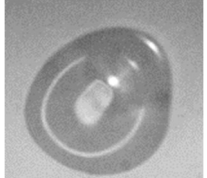
RH (%)	Particle before Poking	Poking	First Frame after Poking	Frame at $\tau_{\text{exp, flow}}$
0	 (a1)		 (a2) 0 Seconds	 (a3) 990 Seconds
25	 (b1)		 (b2) 0 Seconds	 (b3) 6.0 Seconds

Fig. S4. Optical images from poke-flow measurements for a 10 mL extract of a BBOA sample. The images were taken during poke-flow experiments at (a) 0% and (b) 25% RH. Images a1 and b1 correspond to the frames taken before the aerosol particles were poked. Images a2 and b2 correspond to the frames taken right after the particles were poked by the needle. Images a3 and b3 correspond to the time when the equivalent area diameter of the hole had decreased to half of its original diameter (i.e., the experimental flow time, $\tau_{\text{exp, flow}}$).

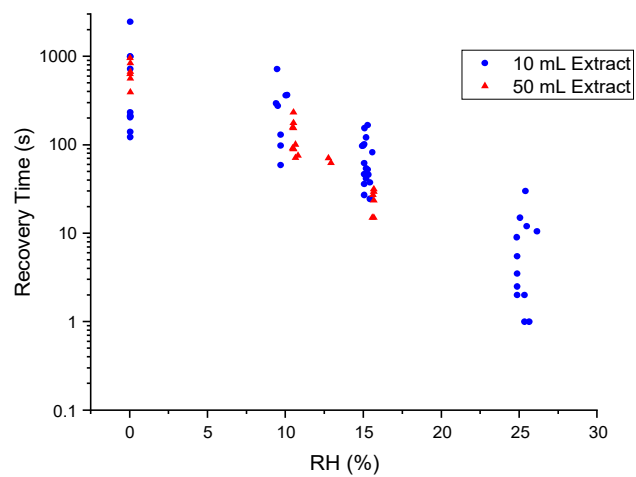


Fig. S5. The experimental recovery times, $\tau_{\text{exp, flow}}$, of the particles after poking as a function of RH for the samples extracted with 10 mL and 50 mL of water. There was no change in recovery time with extraction volume.

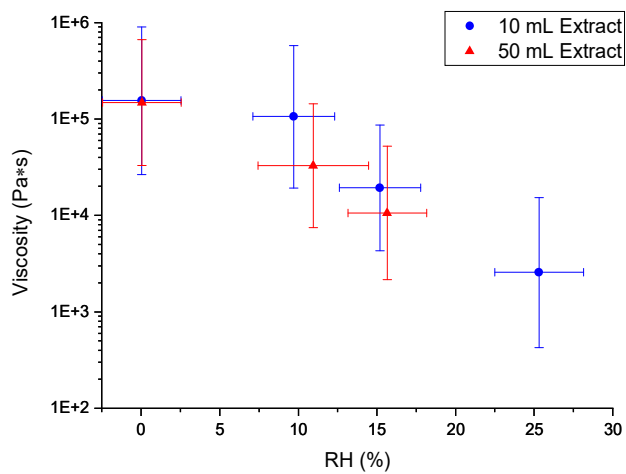


Fig. S6. Derived upper and lower limit viscosities from the recovery times using COMSOL Multiphysics. Symbols show the medians of the viscosity values on a log scale, with y-error bars representing the upper and lower limits at each RH and x-error bars representing the uncertainty in RH. Within the uncertainties of the measurements, the viscosities of the samples with 10 mL and 50 mL of water are the same. As a result, the results for the 10 mL and 50 mL extracts are combined.

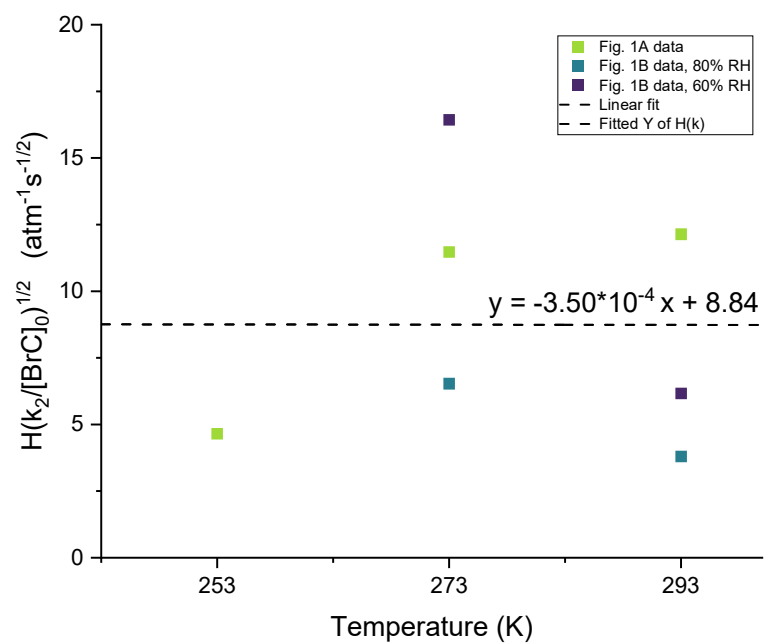


Fig. S7. Values of $H(k_2/[BrC]_0)^{1/2}$ from fitting Eq. 2 to BrC reactivity data from seven flow-tube reactor experiments. The dashed line corresponds to a linear fit of the data ($y = -0.00034x + 8.84$).

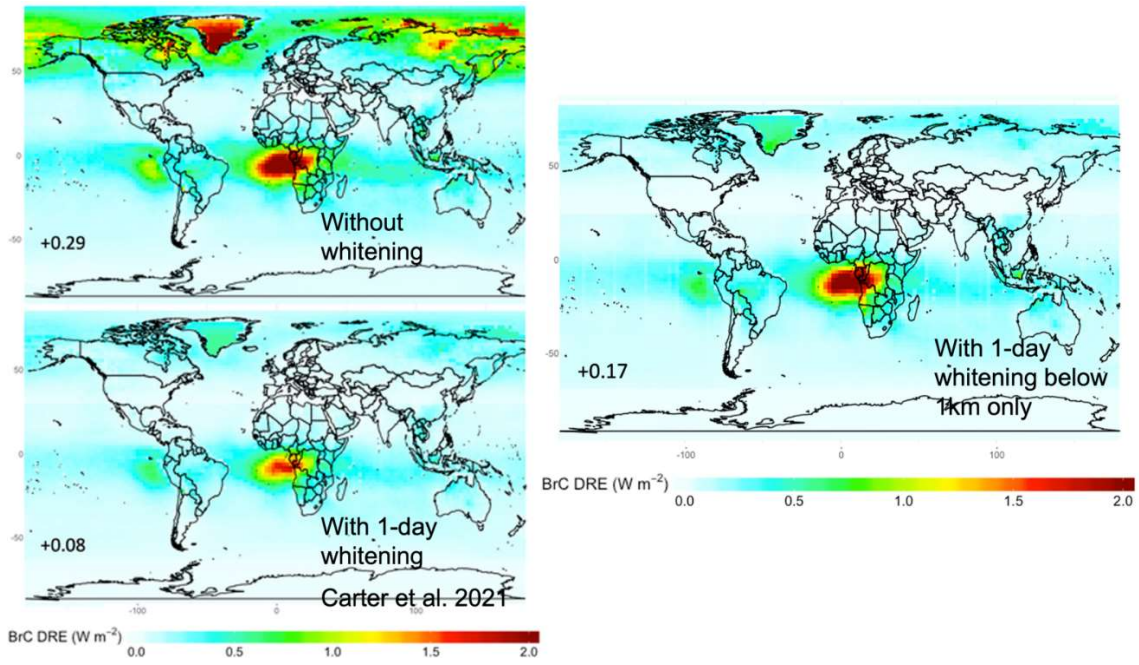


Fig. S8. 2018 annual mean BrC top-of-atmosphere all-sky direct radiative effect.

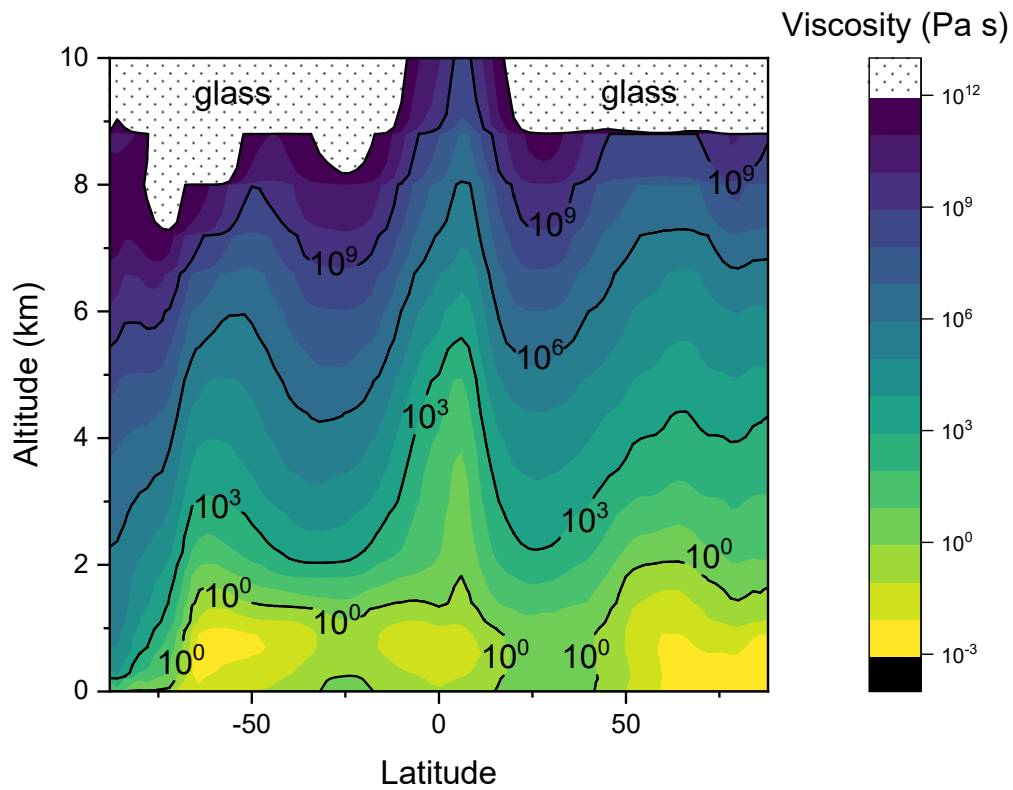


Fig. S9. Global distribution of BBOA viscosities and glass state transitions based on RH and T fields from MERRA2 meteorology.

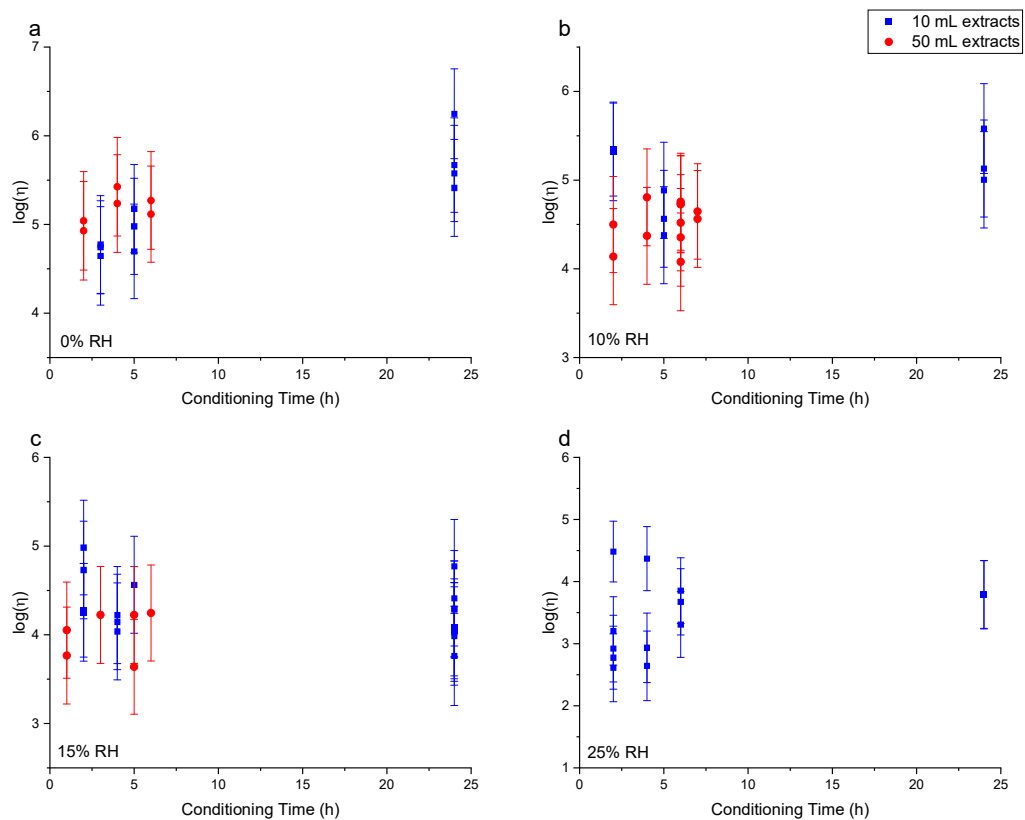


Fig. S10. Viscosities of poked droplets as a function of conditioning time at (a) 0%, (b) 10%, (c) 15%, and (d) 25% RH. Vertical error bars show the upper and lower limits of the derived viscosities, with points representing the midpoint of the upper and lower limits on the log scale. Within the uncertainties of the measurements, the viscosities did not depend on the conditioning time used.

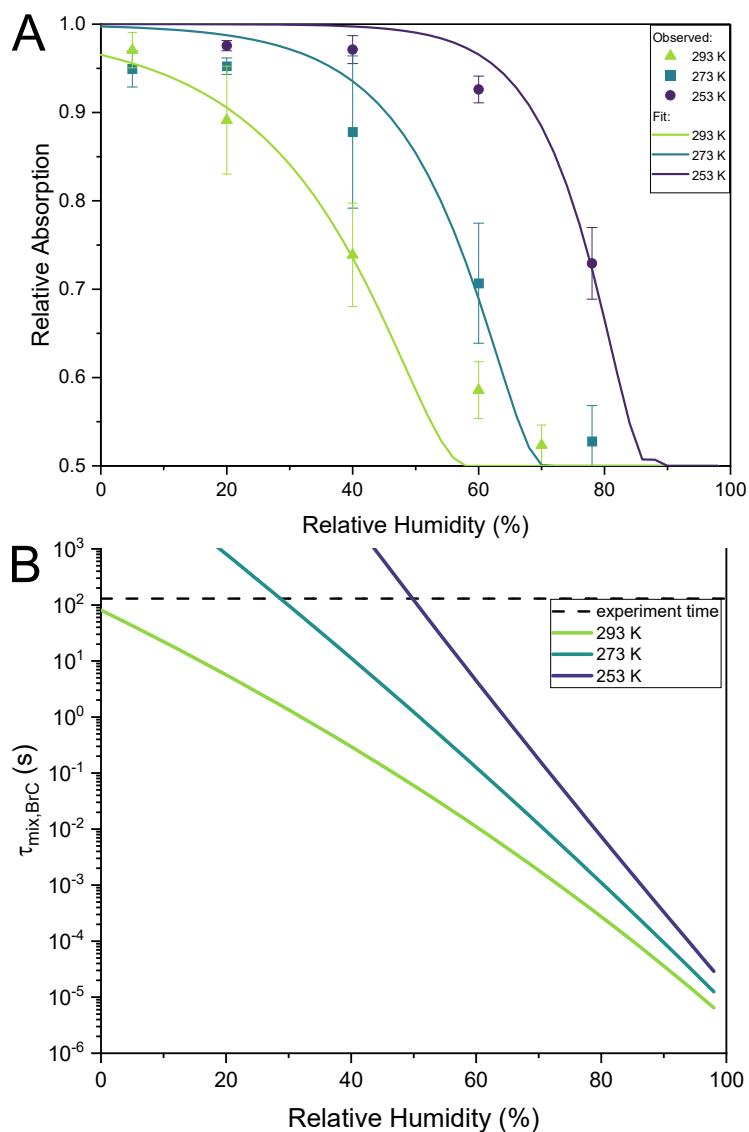


Fig. S11. A) Relative absorption at 405 nm remaining after exposure to 45 ppm of ozone as a function of RH at 253, 273, and 293 K. Error bars represent one standard deviation of four sets of datapoints. The dashed lines correspond to fits to the data assuming the resistor model and the reaction between O_3 and BrC was limited by the fast reaction of O_3 with BrC within a thin shell near the surface. B) Mixing times of BrC within the particles ($\tau_{\text{mix,BrC}}$) as a function of RH at 253, 273, and 293 K calculated with Eq. S12. The dashed black line represents the 130 s residence time of the particles through the flow-tube reactor.

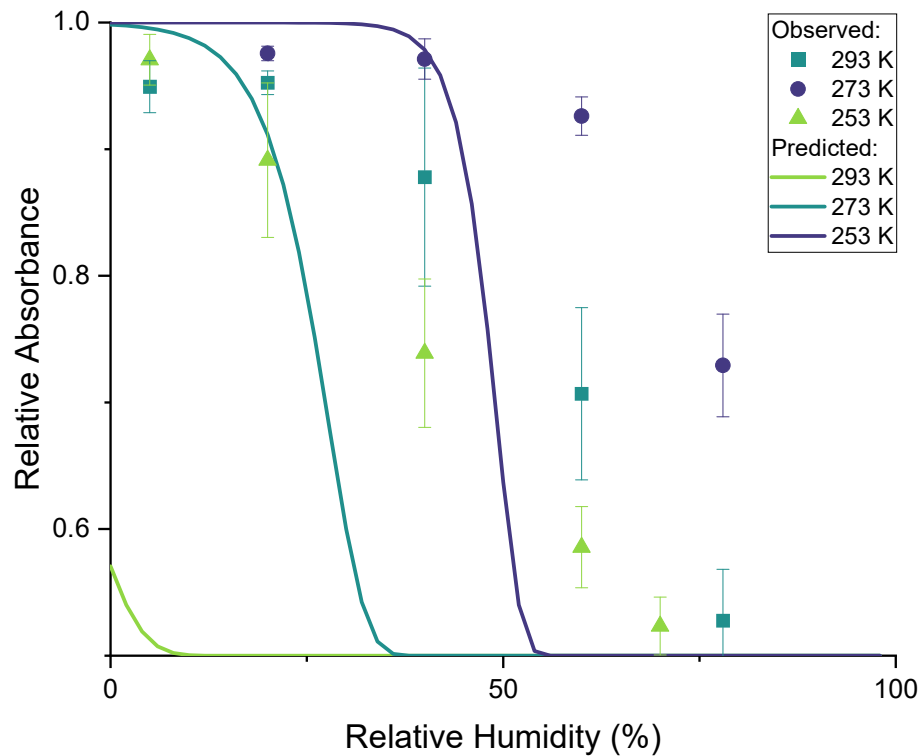


Fig. S12. Relative absorption at 405 nm remaining after exposure to 45 ppm of ozone as a function of RH at 253, 273, and 293 K. Error bars represent one standard deviation of four sets of datapoints. The lines correspond to predictions assuming the reaction between O_3 and BrC occurs at the surface and is limited by only diffusion of BrC to the surface (Eq. S16).

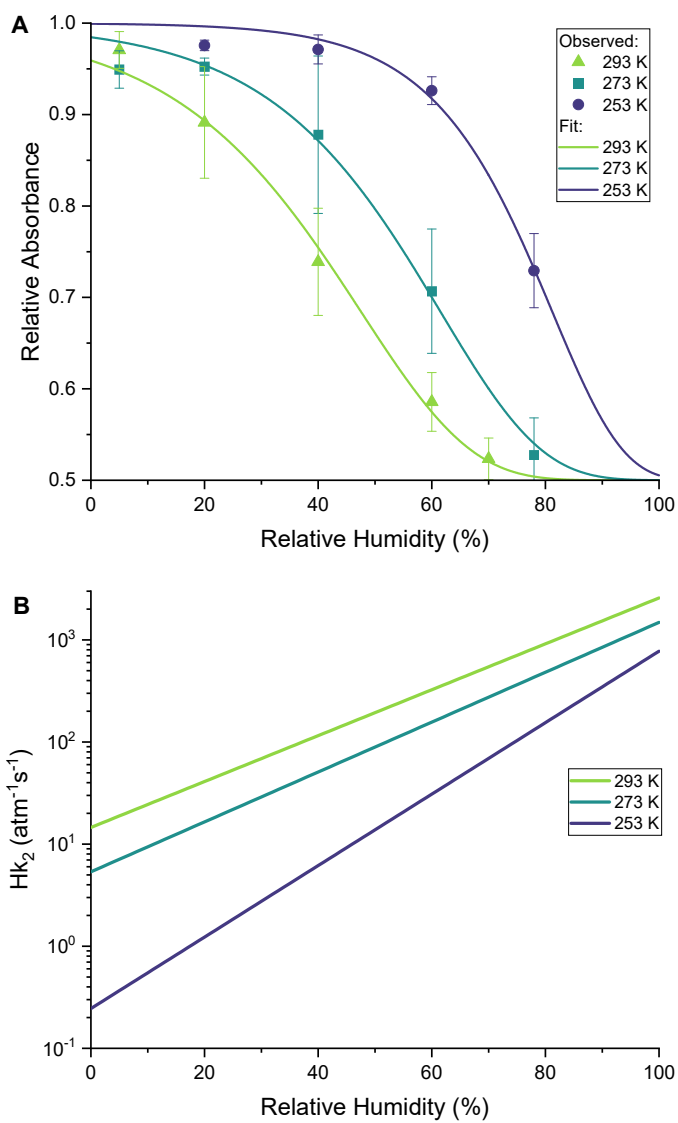


Fig. S13. A) Relative absorption at 405 nm remaining after exposure to 45 ppm of ozone as a function of RH at 253, 273, and 293 K. Error bars represent one standard deviation of four sets of datapoints. The lines correspond to fits to the data assuming the resistor model and O₃ and BrC were well-mixed throughout the particles (Eq. **S18**). B) Values for Hk₂ determined by fitting Eq. **S18** to the experimental data in panel A and assuming the product Hk₂ is an exponential function of RH.

Table S1. COMSOL Multiphysics parameters used when simulating the viscosity of biomass burning aerosol.

	Surface tension (mN m ⁻¹)	Slip length (m)	Density (kg m ⁻³)	Contact angle (°)
Values for lower limit	30 ^a	5×10 ⁻⁹ ^c	1200 ^d	74.4 ^e
Values for upper limit	72.9 ^b	10 ⁻⁶ ^c	1200 ^d	53.6 ^e

^a Giordano et al. (20) and Asa-Awuku et al. (21) observed that the surface tension of the water soluble component of biomass burning aerosol was up to 30% less than pure water. As a conservative lower limit to the surface tension, we used 30 mN m⁻¹, which is consistent with the surface tension of alcohols, organic acids, and esters (22).

^b For a conservative upper limit to the surface tension of our samples we used the surface tension of pure water at 20°C from Vargaftik et al. (23).

^c Slip-length range is based on measurements of slip length of organic compounds and water on hydrophobic surfaces reported in the literature. See Table S2 in Maclean et al. and references therein (24).

^d Density was varied from 1000–1400 kg m⁻³ in the initial simulations and was determined to have no effect upon the simulated viscosity, and hence, a median value of 1200 kg m⁻³ was used.

^e Contact angles were estimated from measurements of the height and radius of individual droplets on the hydrophobic glass slides using a confocal laser scanning microscope.

Table S2. Second order rate constants (k_2) at room temperature for the reaction between O_3 and different types of organic molecules with structures similar to molecules expected for $[BrC]_0$.

Molecule	k_2 ($M^{-1} s^{-1}$)
Shikimic acid ^a	3×10^3
Nitrobenzene ^b	9×10^{-2}
Benzene ^b	2
Toluene ^b	1.4×10^1
4-nitrophenol ^b	$< 5 \times 10^1$
Xylenes ^b	$9 \times 10^1 - 1.4 \times 10^2$
Trimethylbenzenes ^b	$4 - 7 \times 10^2$
Phenol ^b	1.3×10^3
Resorcinol ^b	$> 3 \times 10^5$
Naphthalene ^b	3×10^3
Trans stilbene ^c	3.8×10^5
Triphenylethylene ^c	1.7×10^4
4-tert-butylphenol ^d	3.6×10^4
4-isopropylphenol ^d	3.7×10^4
4-formylphenol ^d	2.6×10^2
4-methoxyphenol ^d	4.7×10^5

^a (25)

^b (26)

^c (27)

^d (28)

SI References

1. L. Korson, W. Drost-Hansen, F. J. Millero, Viscosity of water at various temperatures. *J. Phys. Chem.* **73**, 34–39 (1969).
2. S. Arrhenius, Über die innere Reibung verdünnter wässriger Lösungen. *Zeitschrift für Phys. Chemie* **1**, 285–298 (1887).
3. G. Centeno, G. Sánchez-Reyna, J. Ancheyta, J. A. D. Muñoz, N. Cardona, Testing various mixing rules for calculation of viscosity of petroleum blends. *Fuel* **90**, 3561–3570 (2011).
4. N. E. Rothfuss, M. D. Petters, Characterization of the temperature and humidity-dependent phase diagram of amorphous nanoscale organic aerosols. *Phys. Chem. Chem. Phys.* **19**, 6532–6545 (2017).
5. L. T. Fleming, *et al.*, Molecular composition and photochemical lifetimes of brown carbon chromophores in biomass burning organic aerosol. *Atmos. Chem. Phys.* **20**, 1105–1129 (2020).
6. A. M. Maclean, *et al.*, Global distribution of the phase state and mixing times within secondary organic aerosol particles in the troposphere based on room-temperature viscosity measurements. *ACS Earth Sp. Chem.*
7. M. Shiraiwa, *et al.*, Global distribution of particle phase state in atmospheric secondary organic aerosols. *Nat. Commun.* **8** (2017).
8. C. A. Angell, Liquid fragility and the glass transition in water and aqueous solutions. *Chem. Rev.* **102**, 2627–2650 (2002).
9. C. A. Angell, Relaxation in liquids, polymers and plastic crystals - strong/fragile patterns and problems. *J. Non. Cryst. Solids* **131**, 13–31 (1991).
10. W.-S. W. DeRieux, *et al.*, Predicting the glass transition temperature and viscosity of secondary organic material using molecular composition. *Atmos. Chem. Phys.* **18**, 6331–6351 (2018).
11. J. H. Seinfeld, S. N. Pandis, *Atmospheric chemistry and physics: from air pollution to climate change*, 3rd Ed. (John Wiley & Sons, Inc., 2016).
12. E. Evoy, S. Kamal, G. N. Patey, S. T. Martin, A. K. Bertram, Unified Description of Diffusion Coefficients from Small to Large Molecules in Organic–Water Mixtures. *J. Phys. Chem. A* **124**, 2301–2308.
13. J. W. Morris, *et al.*, Kinetics of submicron oleic acid aerosols with ozone: A novel aerosol mass spectrometric technique. *Geophys. Res. Lett.* **29**, 71-1-71–4 (2002).
14. C. J. Hennigan, *et al.*, Chemical and physical transformations of organic aerosol from the photo-oxidation of open biomass burning emissions in an environmental chamber. *Atmos. Chem. Phys.* **11**, 7669–7686 (2011).
15. J. Chen, *et al.*, A review of biomass burning: Emissions and impacts on air quality, health and climate in China. *Sci. Total Environ.* **579**, 1000–1034 (2017).
16. G. D. Smith, E. Woods, C. L. DeForest, T. Baer, R. E. Miller, Reactive Uptake of Ozone by Oleic Acid Aerosol Particles: Application of Single-Particle Mass Spectrometry to Heterogeneous Reaction Kinetics. *J. Phys. Chem. A* **106**, 8085–8095 (2002).
17. S. D. Razumovskii, G. E. Zaikov, *Ozone and its reactions with organic compounds* (Elsevier Science Publishers, 1984).
18. T. Berkemeier, *et al.*, Ozone uptake on glassy, semi-solid and liquid organic matter and the role of reactive oxygen intermediates in atmospheric aerosol chemistry. *Phys. Chem. Chem. Phys.* **18**, 12662–12674 (2016).
19. J. W. Grayson, M. Song, M. Sellier, A. K. Bertram, Validation of the poke-flow technique combined with simulations of fluid flow for determining viscosities in samples with small volumes and high viscosities. *Atmos. Meas. Tech.* **8**, 2463–2472 (2015).
20. M. R. Giordano, D. Z. Short, S. Hosseini, W. Lichtenberg, A. A. Asa-Awuku, Changes in Droplet Surface Tension Affect the Observed Hygroscopicity of Photochemically Aged Biomass Burning Aerosol". *Environ. Sci. Technol.* **47**, 10980–10986 (2013).
21. A. Asa-Awuku, A. P. Sullivan, C. J. Hennigan, R. J. Weber, A. Nenes, Investigation of molar volume and surfactant characteristics of water-soluble organic compounds in biomass burning aerosol. *Atmos. Chem. Phys.* **8**, 799–812 (2008).

22. A. H. Demond, A. S. Lindner, Estimation of interfacial tension between organic liquid mixtures and water. *Environ. Sci. Technol.* **27**, 2318–2331 (1993).
23. N. B. Vargaftik, B. N. Volkov, L. D. Voljak, International Tables of the Surface Tension of Water. *J. Phys. Chem. Ref. Data* **12**, 817–820 (1983).
24. A. M. Maclean, *et al.*, Humidity-Dependent Viscosity of Secondary Organic Aerosol from Ozonolysis of β -Caryophyllene: Measurements, Predictions, and Implications. *ACS Earth Sp. Chem.* **5**, 305–318 (2021).
25. S. S. Steimer, M. Lampimaki, E. Coz, G. Grzinic, M. Ammann, The influence of physical state on shikimic acid ozonolysis: a case for in situ microspectroscopy. *Atmos. Chem. Phys.* **14**, 10761–10772 (2014).
26. J. Hoigné, H. Bader, Rate constants of reactions of ozone with organic and inorganic compounds in water—I. *Water Res.* **17**, 173–183 (1983).
27. H. Henry, M. Zador, S. Fliszár, A Quantitative Investigation of the Ozonolysis Reaction. XVIII. A Kinetic Study of the Ozone Attack on Phenylethylenes. *Can. J. Chem.* **51**, 3398–3402 (1973).
28. P. R. Tentscher, M. Bourgin, U. von Gunten, Ozonation of Para-Substituted Phenolic Compounds Yields p-Benzoquinones, Other Cyclic α,β -Unsaturated Ketones, and Substituted Catechols. *Environ. Sci. Technol.* **52**, 4763–4773 (2018).